Journal of ELECTRONIC MATERIALS
DOI: 10.1007/s11664-010-1375-1

Empirical Study of Hall Bars on Few-Layer Graphene on C-Face 4H-SiC

M.L. BOLEN,[1,2,5] T. SHEN,[1,4] J.J. GU,[1,2] R. COLBY,[1,3] E.A. STACH,[1,3] P.D. YE,[1,2] and M.A. CAPANO[1,2]

1.—Birck Nanotechnology Center, Purdue University, West Lafayette, IN 47907, USA. 2.—School of Electrical and Computer Engineering, Purdue, University, West Lafayette, IN 47907, USA. 3.—School of Materials Engineering, Purdue, University, West Lafayette, IN 47907, USA. 4.—Department of Physics, Purdue University, West Lafayette, IN 47907, USA. 5.—e-mail: mbolen@purdue.edu

Hall bars were fabricated on epitaxial graphene formed on 4H-SiC{0001} under various growth environments. Subsequently, they were analyzed via electrical characterization, atomic force microscopy (AFM), Raman mapping, and transmission electron microscopy (TEM) with emphasis on the C-face. The results of the measurement techniques were then corroborated to find correlations. It was found that there is a positive correlation between Hall mobility values and growth pressure in an Ar environment for the C-face. AFM elucidated that topographic features do not correlate with Hall mobility values, nor does device height correlate with carrier concentration. Raman spectroscopy showed that there is a correlation between Hall mobility values and the 2D peak full-width at half-maximum, and a weak correlation with 2D peak position. Additionally, the spectra are sensitive to topographic changes and film discontinuities. Dark-field TEM found higher levels of contrast variation in the SiC⟨0001⟩ direction, representative of out-of-plane disorder, corresponding to a blue-shift in the 2D peak position. This disorder does not seem to strongly influence Hall mobility values, as it was found in the device with the highest measured Hall mobility: 18,700 $cm^2\ V^{-1}\ s^{-1}$.

Key words: Graphene, Hall mobility, atomic force microscopy, Raman spectroscopy, transmission electron microscopy

INTRODUCTION

With its simple, yet fascinating, two-dimensional honeycomb-like lattice, graphene has been at the heart of a growing amount of research. A broad range of applications have been envisioned as end-uses of graphene,[1] but each depends on having a reproducible and reliable means to manufacture graphene. To this end, the use of thermal desorption of Si from SiC to form epitaxial graphene (EG) is a promising technique;[1–4] however, there is still much to be learned about the correlation between growth conditions and electronic properties. Prior studies have focused mainly on the Si-face,[2,5,6] which is surprising given the nearly order of magnitude increase in Hall mobility that the C-face offers over the Si-face. An initial attempt at explaining the differences in mobility between the polar faces has been reported by Robinson et al.[6] This manuscript presents findings of the parameters that do and do not affect the Hall mobility of EG, with particular focus on the C-face. Deeper understanding of the causes of mobility variation will be important to reach terahertz devices fabricated on EG.

EXPERIMENTAL PROCEDURES

The starting material was nominally on-axis, semi-insulating 4H-SiC wafers, purchased from Cree and chemomechanically polished by NovaSiC. The wafers were diced, and samples were cleaned with solvents, a piranha bath (1:1—H_2SO_4:H_2O_2),

(Received July 14, 2010; accepted August 25, 2010)

Published online: 14 September 2010

and buffered oxide etch before being loaded into an Epigress VP508 hot-wall chemical vapor deposition system. After loading, sample surfaces were etched in a hydrogen environment at 1500°C for 10 min. The temperature inside the system was measured with a Heitronics two-color pyrometer. After cleaning, EG was formed by ramping the temperature of the chamber at a fixed rate to 1600°C in vacuum (10^{-5} mbar) or Ar ambient (1 mbar to 300 mbar). The samples were held at the 1600°C growth temperature for 10 min. For each growth reported, a Si-face and a C-face sample were grown together at the same time under the exact same conditions.

After the growth, ungated Hall bars of identical size (22 μm × 10 μm) were fabricated on the samples using standard photolithographic techniques with AZ1518 and AZ1805 photoresists and Ti contacts with Au caps. The Hall bars were isolated through the use of an O_2 plasma etch. After fabrication, a current–voltage sweep was performed between contact pads to ensure ohmic contacts to the graphene had been formed. Then, a standard alternating-current (AC) lock-in technique was used to measure the Hall resistance as a function of magnetic field. The magnetic field was swept between −0.2 T and 0.2 T with a current in the single microamps range. All reported Hall mobility values were taken at room temperature.

The samples were analyzed before and after Hall bar fabrication with a Veeco Dimension 3100 atomic force microscope (AFM) in dynamic contact mode with Veeco's TESP model uncoated Si microcantilevers. Raman mapping was performed with a HORIBA Jobin Yvon XploRA at a wavelength of 532 nm, power under 4 mW, and lateral resolution of 600 nm. Finally, selected device areas were prepared for cross-sectional transmission electron microscopy (TEM) using a focused ion beam (FIB) liftout method on an FEI Nova dual-beam FIB/SEM, equipped with a Klöcke nanomanipulator.[7] Protective layers of Pt/C were deposited locally, first with the electron beam to avoid surface damage, then followed by a thicker layer deposited using the ion source. TEM images were obtained with an FEI Titan 80-300 operating at 300 kV or an FEI Tecnai T20 at 80 kV.

RESULTS AND DISCUSSION

The measured Hall mobility values for both C-face and Si-face devices are presented in Fig. 1. The positive correlation between growth pressure and mobility for the C-face is similar to that found by Tedesco et al.[8] This correlation continues to the point where a large enough Ar overpressure inhibits Si desorption from the SiC sample and EG formation is halted. At 100 mbar (50 mbar) and 10 min growth time, AFM and Raman spectroscopy indicate there is no longer a continuous film of EG on the C-face (Si-face) surface. Instead, on the C-face, isolated patches of EG are found at random locations across

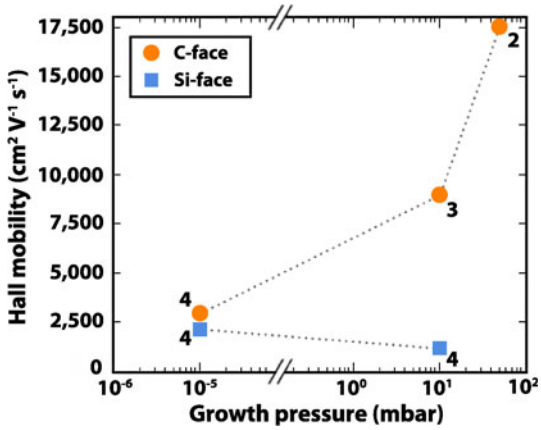

Fig. 1. Average room-temperature Hall mobility values versus pressure for both C-face and Si-face devices. The graphene coverage is discontinuous at pressures above 50 mbar for the C-face and 10 mbar for the Si-face. The *number* next to each point represents the number of devices tested, and the *dotted lines* serve as guides to the eye.

the surface. With increased growth time, it is expected, based on previous research, that a continuous film would be achieved at 100 mbar;[4] but for this work, growth time is held constant at 10 min.

There is not a clear increase in Hall mobility values as pressure increases on the Si-face, unlike the trend other groups have observed.[2,3] This discrepancy could be caused by an increasing density of discontinuities in our EG film. As growth pressure increases, so too does the suppression of Si desorption, which leads to a discontinuous EG film. Thus, there is a decrease in the percentage of the surface which is covered by EG as growth pressure increases. This notion is confirmed via AFM phase-contrast imaging (not shown).[4,9] These discontinuities serve as scattering sites, thereby lowering the overall measured Hall mobility. From the experimental growth conditions reported by others, their growth times are longer than 10 min, which increases surface coverage and decreases inhomogeneous discontinuities. Even with these discontinuities, the average Hall bar mobility values for the Si-face in this work are found to be twice as high as those reported elsewhere.[2,3]

AFM Study

After mobilities were measured, each device was analyzed with AFM. This provides a topographical analysis to determine whether ridges play a role in electrical variations. It is known that EG has a tendency to form ridges due to the coefficient of thermal expansion mismatch between 4H-SiC and EG.[10] What is not known is how much these ridges affect electrical characteristics. The disturbance of the graphene lattice by a ridge should create carrier scattering sites. To study this, densities of ridges and ridge nodes were counted, and the ridge type was characterized.

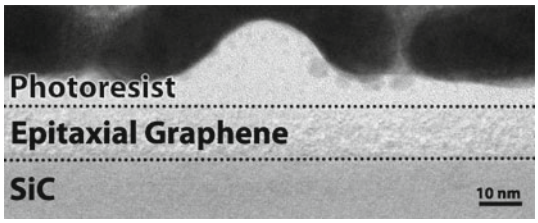

Fig. 2. Cross-sectional TEM image showing a "spurious" ridge which is not conformal to the underlying EG film. *Dotted lines* emphasize material interfaces. Image acquired at 300 kV.

There are two types of ridges that are intrinsic to the surface of EG. The first type are primary ridges, which are defined as ridges that maintain their height between ridge nodes (defined by the intersection of two or more ridges). The other type is referred to as secondary ridges, which start at a node and decrease in height as a function of distance away from the node. A secondary ridge will eventually taper into smooth graphene regions to the point of becoming indistinguishable. This nomenclature follows that used in Prakash et al.[10]

Not all ridges found on fabricated Hall bars are intrinsic to EG. Through TEM and AFM analysis, a number of ridges were found to be contained in a thin film above the EG which is mostly conformal but that forms spurious ridges at locations not determined by the underlying EG. This film is believed to be residual photoresist left following device fabrication, as seen in Fig. 2. In this figure, photoresist is shown to form a mound that appears as a ridge in a cross-sectional TEM image. Ridges in the photoresist layer are referred to as "spurious." An example of both types of ridges in an AFM micrograph can be seen in Fig. 7a. To distinguish between intrinsic ridges caused by the thermal coefficient mismatch in the graphene–SiC system and spurious ridges, AFM profilometry was used. For an intrinsic ridge, the ratio of ridge arc length to base width is nearly an order of magnitude greater than the corresponding ratio for a spurious ridge. The well-pronounced spurious ridges have an average ratio of arc length to base of 0.006, whereas the average ratio for the intrinsic ridges (measured before Hall bar fabrication) was found to be 0.05.

Using this distinction between intrinsic and spurious ridges, the average number of intrinsic primary and secondary ridges and ridge nodes per Hall bar was counted and is plotted against Hall mobility in Fig. 3. Initial results showed no correlation between Hall mobility values and the number of primary or secondary ridges, the number of nodes, or any ratio of the three variables. This implies that carrier scattering is not dependent on these surface features. Instead, a different scattering mechanism is dominating over ridge-associated scattering events. No consideration was given to the orientation of ridges with regard to the Hall bar. In a second set of calculations, average ridge and node densities of each growth condition were calculated from AFM micrographs taken before Hall bar fabrication. These values also appear to provide no predictive insight into resulting Hall mobility.

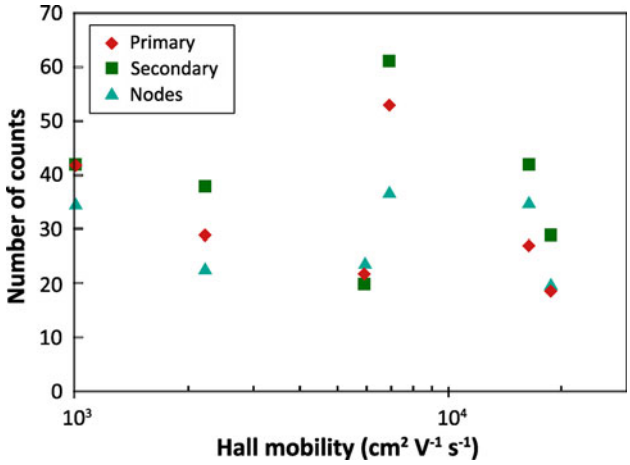

Fig. 3. The number of intrinsic ridges and nodes, as counted via AFM profilometry, does not show any correlation with the respective device's Hall mobility value.

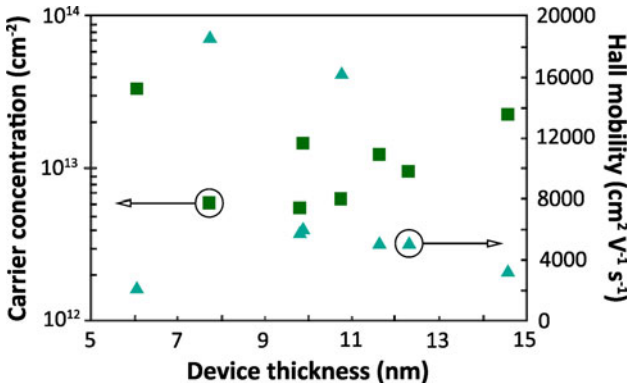

Fig. 4. There is no apparent correlation between the thickness of a Hall bar and its measured Hall mobility or carrier concentration. This implies that there is not equal conduction from each graphene layer in the film.

Measured device thickness from AFM can be compared against the measured Hall mobility and carrier concentration values. To calculate device thickness, 9 nm was subtracted from the measured AFM height between the top of the Hall bar and the SiC substrate. This offset represents the average thickness of the photoresist covering the Hall bars as found from cross-sectional TEM. Figure 4 shows an apparent lack of correlation between the thickness of each device and its Hall mobility and carrier concentration value. This is important, because it implies that each graphene layer within the EG does not contribute equally to conduction. If there were equal conduction, then for each additional layer, there would be a monotonic increase in carrier concentration with thickness. Correspondingly, there would be a decrease in the Hall mobility value,

since carrier concentration and Hall mobility are inversely related. Instead, neither of these trends are apparent in Fig. 4.

Raman Spectroscopic Study

The second method used to characterize the Hall bars was Raman spectroscopy. This technique has shown graphene to be very sensitive to variations in laser excitation energy,[11,12] film thickness,[13–16] carrier density,[17–20] and strain.[21–23] This multivariate dependence makes interpretation of Raman spectroscopic data difficult, since all three film-dependent variables could be changing independently of each other, but be convoluted together in the Raman spectrum. A formal treatment of these variables is beyond the scope of this work and will be addressed in a future manuscript.

For this study, Raman mapping is used to find spatial variations in graphene's signature peaks, the G (1600 cm^{-1}) and 2D (2680 cm^{-1}) peaks. Both peak position and full-width at half-maximum (FWHM) of the peaks were analyzed for each Raman spectrum. In addition, the average peak position and FWHM of a device were calculated from all spectra of the Raman map. More importance is given to 2D peak variations due to the fact that the G peak is convoluted with background SiC resonant peaks at 1520 cm^{-1} and 1710 cm^{-1}. This makes accurate separation of the G peak from the background a challenge. Additionally, it is found that the G peak does not vary in wavenumber as much as the 2D peak. This can be seen in the Raman map shown in Fig. 5. The 2D peak position and FWHM values shown in Fig. 5b and c have a much larger range as compared with the G peak position and FWHM shown in Fig. 5d and e. This gives the 2D peak better resolution for detecting changes in EG thickness, carrier concentration variations, and strain nonuniformities.

Figure 5 also shows how topographic features corroborate with Raman spectra. The original AFM profilometry micrograph is shown in Fig. 5a. The Raman maps in Fig. 5b–e are the results of an automated analysis of each individual Raman spectrum. The mapped spectra are then made partially transparent and overlaid on the dotted section from Fig. 5a. This provides a more convenient method of visually interpreting how the topography of the Hall bar affects Raman spectra. This particular Hall bar is chosen because of the discontinuities, as evidenced by the relatively deep holes in Fig. 5a, in the EG film. These are not common features in our films, but serve as points of reference in the Raman map. In Fig. 5b, there are two interesting observations to be made. First is that around the discontinuities a lower wavenumber is found for the 2D peak position, but this has little bearing on the FWHM of the peak, as seen in Fig. 5c. Additionally, it is found that the G peak position shows a blue-shift at the discontinuities, as evidenced in Fig. 5d. The second interesting feature is the blue-shifted right side of the EG, in Fig. 5b, which is separated by intrinsic ridges from the left, comparatively lower-wavenumber side of the EG. As stated above, there are multiple possible reasons for these changes in Raman spectra. A blue-shift in the G peak could be caused from compressive strain in the film or an increase in either hole or electron carrier

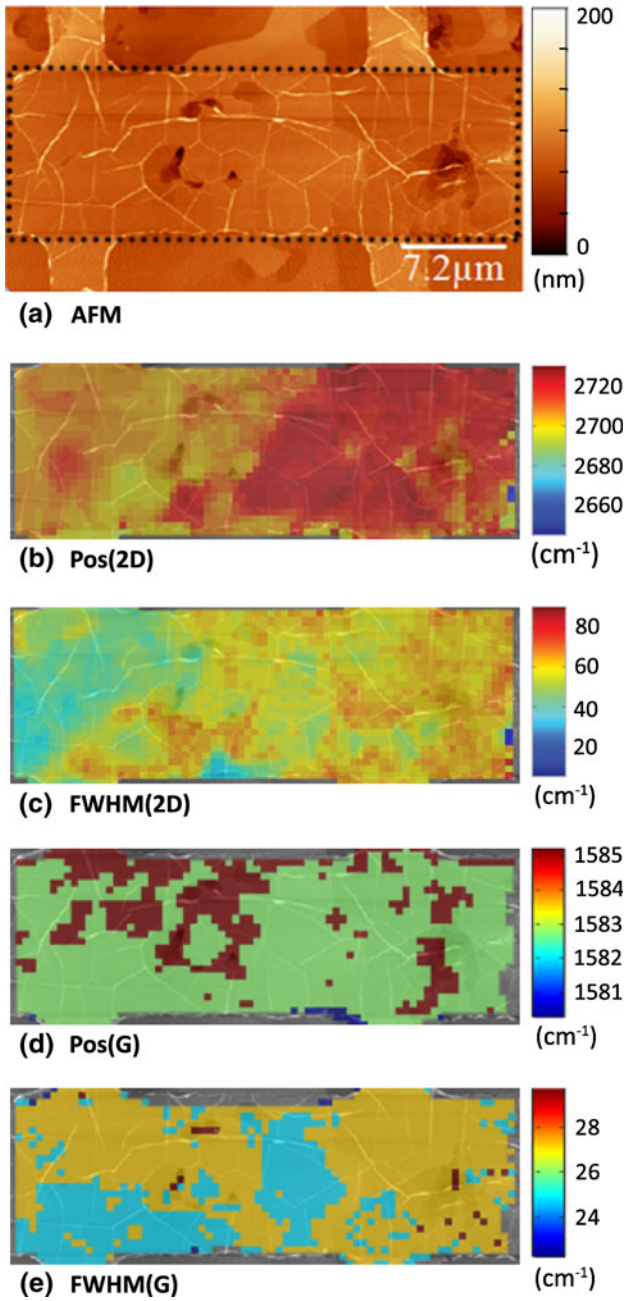

Fig. 5. (a) AFM profilometry micrograph of a Hall bar showing ridges and nonuniformities in the EG as evidenced by deep pits. The *dotted region* highlights where the Raman mapping is performed. Spatial Raman spectra are analyzed and overlaid onto a cropped and grayscaled AFM micrograph from (a) to show correlations between topographic features and peak variations. The Raman maps correspond to (b) 2D peak position, (c) 2D peak FWHM, (d) G peak position, and (e) G peak FWHM.

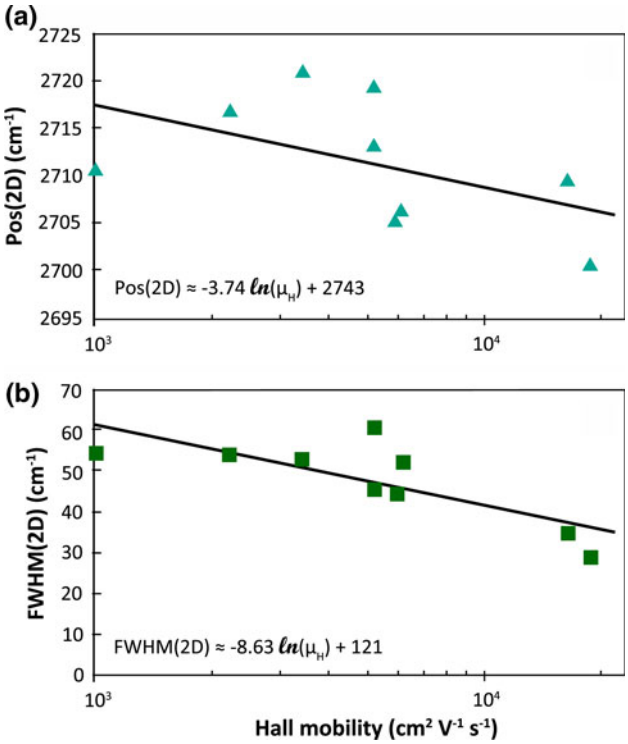

Fig. 6. A negative correlation is evidenced between Hall mobility values and both the average (a) 2D peak position and (b) 2D FWHM of Hall bars.

concentration. A blue-shift in the 2D peak could come from a thicker film (assuming there is some degree of electronic coupling between layers), compressive strain in the film, or an increase in the hole carrier concentration.

Using averages from the mapping of the G and 2D peak position and FWHM, it is found that there is a weak correlation between the average FWHM and position of the 2D peak and a device's Hall mobility value. Figure 6 evidences the negative correlation with both peak position and FWHM. For each data point in Fig. 6, thousands of spectra are averaged together for devices that have been mapped by Raman spectroscopy, and a minimum of 30 spectra are collected for devices that have not been Raman mapped. With a correlation coefficient, R^2, of 0.59, as compared with 0.25, it is found that the 2D FWHM provides more predictive insight into the Hall mobility value as compared with the 2D peak position. The 2D FWHM correlation is similar to that found by Robinson et al.,[6] except that 2D FWHM uniformity is not used to segment the data. Instead, all data points in Fig. 6 are plotted without distinguishing their uniformity. Increases in the 2D FWHM can be attributed to an increase in the thickness of the EG or to strain.

TEM Study

Greater insight into the structure of EG is gained through analysis of dark-field TEM images taken

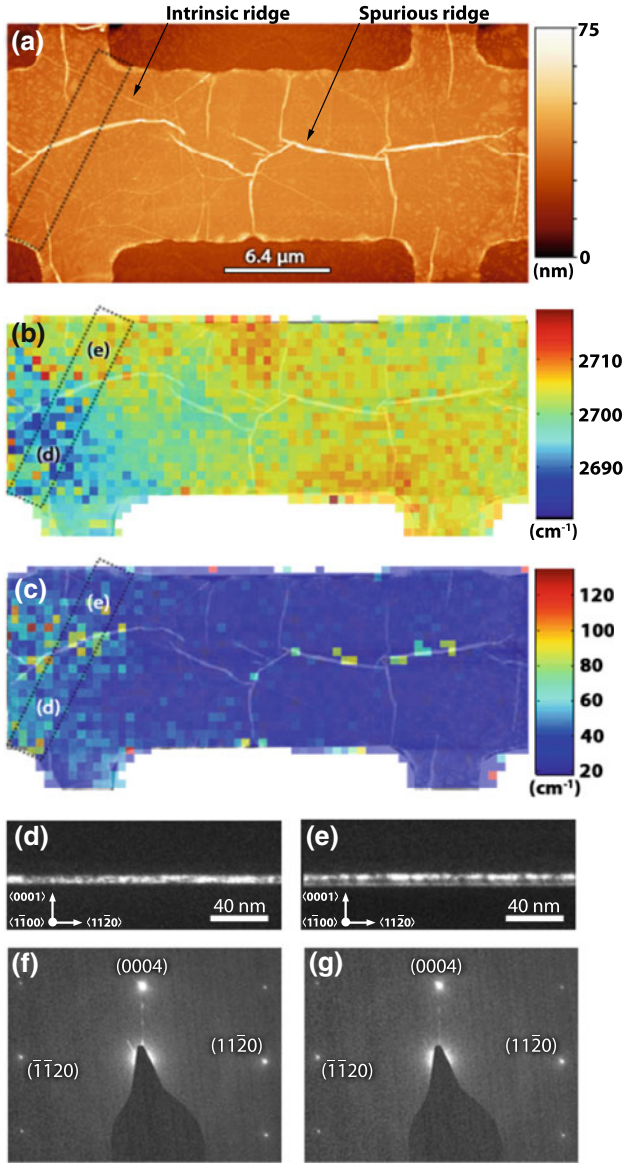

Fig. 7. (a) AFM profilometry micrograph showing Hall bar with mobility of 18,700 cm^2 V^{-1} s^{-1} and (b) Raman map of 2D peak position and (c) 2D FWHM from the same Hall bar overlaid on the image from (a). The *dotted inset boxes* outline a section removed via FIB and subsequently imaged via TEM, as seen in (d) and (e), using indirect dark-field conditions, indicated in the selected-area diffraction patterns of (f) and (g), respectively. The 4H-SiC reflections in (f) and (g) are indexed as a reference.

from regions with variations in the 2D peak position in the Raman map, denoted as (d) and (e), in Fig. 7b. To explore the interplay between the Raman spectra and TEM information, Fig. 7b shows a dotted region where a section of both the EG and underlying SiC substrate is examined in cross-section by TEM. The film is 16 graphene layers thick, which corresponds to a thickness of 5 nm. Additionally, the thickness is uniform throughout the entire film, except at a single intrinsic ridge which is identified in Fig. 7a. The film is imaged at 300 kV under indirect dark-field conditions aligned along $\langle 1\bar{1}00 \rangle$ relative to the

SiC substrate using a 10 μm objective aperture placed between the direct beam and the 4H-SiC(0004) reflection. The resulting dark-field images are sensitive to changes of (0001) reflections of the EG film. For comparison with the 2D peak position, the 2D FWHM Raman map is also shown in Fig. 7c. The changes in FWHM are not as drastic as those in the peak position.

As can be seen in Fig. 7d and e, there are lateral variations in contrast, along the SiC$\langle 11\bar{2}0\rangle$ direction, across the entire EG film. While this can be partially attributed to minor surface damage introduced during TEM sample preparation, it may also be a result of local disorder in the EG or rotations of the EG surface normal away from SiC$\langle 0001\rangle$. Selected-area diffraction patterns, as seen in Fig. 7f and g, acquired from the regions in Fig. 7d and e, respectively, at 80 kV, suggest that the strong variations in contrast in the $\langle 0001\rangle$ direction in Fig. 7e are the result of rotations of the EG planes of the film about the $\langle 11\bar{2}0\rangle$ direction relative to the SiC substrate. The sharpness of the {0001}-type EG reflections confirms that the contrast change from Fig. 7d and e is not a result of large-scale rotations about SiC$\langle 1\bar{1}00\rangle$. Comparing dark-field TEM images in Fig. 7d and e, the contrast changes more frequently and abruptly in Fig. 7e. This conclusion is consistent with the Raman data that shows variations in the 2D peak position in region (e) which is blue-shifted as compared with region (d). Of further interest is that this particular Hall bar has Hall mobility of 18,700 $cm^2\ V^{-1}\ s^{-1}$ despite these nonuniformities evidenced by both TEM and Raman spectroscopy.

CONCLUSIONS

Hall mobility values were measured on EG grown under various environments and growth pressures on the C-face and Si-face of 4H-SiC. Mobility values were measured, with a maximum of 1900 $cm^2\ V^{-1}\ s^{-1}$ for growth under high vacuum on the Si-face and 18,700 $cm^2\ V^{-1}\ s^{-1}$ for growth under 50 mbar Ar on the C-face. The C-face shows a positive correlation between Hall mobility and growth pressure. AFM study elucidates that topographic features do not correlate with Hall mobility values, nor does device height correlate with carrier concentration. This implies that other scattering events are dominating over ridge-associated scattering and that each graphene layer does not contribute equally to conduction, respectively. Raman mapping study shows that there is a correlation between Hall mobility values and 2D peak FWHM, and a weak correlation with 2D peak position. Additionally, the spectra are sensitive to topographic changes, as evidenced through correlation between discontinuities in the film and the 2D and G peak positions. Finally, dark-field TEM study finds higher levels of contrast variation in the SiC$\langle 0001\rangle$ direction, representative of out-of-plane disorder, corresponding to a blue-shift in the 2D peak position. This disorder does not seem to strongly influence Hall mobility values.

ACKNOWLEDGEMENTS

We wish to acknowledge Prof. Yong Chen and Luis Jauregui for Raman usage. This work is funded through Indiana's 21st Century Fund, the Defense Advanced Research Projects Agency, and the United States Air Force.

REFERENCES

1. A.K. Geim and K.S. Novoselov, *Nat. Mater.* 6, 183 (2007).
2. K.V. Emtsev, A. Bostwick, K. Horn, J. Jobst, G.L. Kellogg, L. Ley, J.L. McChesney, T. Ohta, S.A. Reshanov, J. Röhrl, E. Rotenberg, A.K. Schmid, D. Waldmann, H.B. Weber, and T. Seyller, *Nat. Mater.* 8, 203 (2009).
3. J.L. Tedesco, B.L. VanMil, R.L. Myers-Ward, J.M. McCrate, S.A. Kitt, P.M. Campbell, G.G. Jernigan, J.C. Culbertson, J.C.R. Eddy, and D.K. Gaskill, *Appl. Phys. Lett.* 95, 122102 (2009).
4. M.L. Bolen, S.E. Harrison, L.B. Biedermann, and M.A. Capano, *Phys. Rev. B* 80, 115433 (2009).
5. C. Virojanadara, M. Syväjarvi, R. Yakimova, L.I. Johansson, A.A. Zakharov, and T. Balasubramanian, *Phys. Rev. B* 78, 245403 (2008).
6. J.A. Robinson, M. Wetherington, J.L. Tedesco, P.M. Campbell, X. Weng, J. Stitt, M.A. Fanton, E. Frantz, D. Snyder, B.L. VanMil, G.G. Jernigan, R.L. Myers-Ward, C.R. Eddy, and D.K. Gaskill, *Nano Lett.* 9, 2873 (2009).
7. R.M. Langford and C. Clinton, *Micron* 35, 607 (2004).
8. J.L. Tedesco, B. VanMil, R.L. Myers-Ward, J. Culbertson, G. Jernigan, P. Campbell, J.M. McCrate, S.A. Kitt, C.E. Jr., and D.K. Gaskill, *ECS Trans.* 19, 137 (2009).
9. T. Ohta, N.C. Bartelt, S. Nie, K. Thürmer, and G.L. Kellogg, *Phys. Rev. B* 81, 121411 (2010).
10. G. Prakash, M.A. Capano, M.L. Bolen, D. Zemlyanov, and R.G. Reifenberger, *Carbon* 48, 2383 (2010).
11. R.P. Vidano, D.B. Fischbach, L.J. Willis, and T.M. Loehr, *Solid State Commun.* 39, 341 (1981).
12. L.M. Malard, J. Nilsson, D.C. Elias, J.C. Brant, F. Plentz, E.S. Alves, A.H. Castro Neto, and M.A. Pimenta, *Phys. Rev. B* 76, 201401(R) (2007).
13. D. Graf, F. Molitor, K. Ensslin, C. Stampfer, A. Jungen, C. Hierold, and L. Wirtz, *Nano Lett.* 7, 238 (2007).
14. C. Faugeras, A. Nerrière, M. Potemski, A. Mahmood, E. Dujardin, C. Berger, and W.A. de Heer, *Appl. Phys. Lett.* 92, 011914 (2008).
15. A. Gupta, G. Chen, P. Joshi, S. Tadigadapa, and P.C. Eklund, *Nano Lett.* 6, 2667 (2006).
16. A.C. Ferrari, J.C. Meyer, V. Scardaci, C. Casiraghi, M. Lazzeri, F. Mauri, S. Piscanec, D. Jiang, K.S. Novoselov, S. Roth, and A.K. Geim, *Phys. Rev. Lett.* 97, 187401 (2006).
17. A. Das, S. Pisana, B. Chakraborty, S. Piscanec, S.K. Saha, U.V. Waghmare, K.S. Novoselov, H.R. Krishnamurthy, A.K. Geim, A.C. Ferrari, and A.K. Sood, *Nat. Nanotechnol.* 3, 210 (2008).
18. J. Yan, Y. Zhang, P. Kim, and A. Pinczuk, *Phys. Rev. Lett.* 98, 166802 (2007).
19. S. Pisana, M. Lazzeri, C. Casiraghi, K.S. Novoselov, A.K. Geim, A.C. Ferrari, and F. Mauri, *Nat. Mater.* 6, 198 (2007).
20. V.N. Popov and P. Lambin, *Phys. Rev. B.* 82, 045406 (2010).
21. T.M.G. Mohiuddin, A. Lombardo, R.R. Nair, A. Bonetti, G. Savini, R. Jalil, N. Bonini, D.M. Basko, C. Galiotis, N. Marzari, K.S. Novoselov, A.K. Geim, and A.C. Ferrari, *Phys. Rev. B*, 79, 205433 (2009).
22. T. Yu, Z. Ni, C. Du, Y. You, Y. Wang, and Z. Shen, *J. Phys. Chem. C* 112, 12602 (2008).
23. G. Tsoukleri, J. Parthenios, K. Papagelis, R. Jalil, A.C. Ferrari, A.K. Geim, K.S. Novoselov, and C. Galiotis, *Small* 5, 2397 (2009).